Study of Oscillating Blades from Stable to Stalled Conditions

Barakos, G.[*]
University of Glasgow
Department of Aerospace Engineering
Glasgow G12 8QQ
United Kingdom
Tel: + 44 141 330 6465
Fax: + 44 141 330 5560
Email: gbarakos@aero.gla.ac.uk

Johansson, U.[†]
Volvo Aero Corporation
Aerothermodynamics
SE-461 81 Trollhättan
Sweden
Tel: + 46 520 937 62
Fax: + 46 520 985 21
Email: ulf.j.johansson@volvo.com

Svensdotter.S.[††]
Rolls-Royce Plc
Defence Aerospace
Bristol BS34 7QE
United Kingdom
Tel: + 44 117 97 95 311
Fax: + 46 117 97 95 286
Email: susanne.svensdotter@rolls-royce.com

Authors' names in alphabetical order
[*] PhD, Lecturer
[†] MSc, Test Engineer
[††] PhD, Technology Engineer

Abstract

This paper presents comparisons between measured and predicted pressure stability on the suction side of an oscillation blade at an inlet Mach number of 0.5, with oscillation frequencies from 60 to 210Hz, mean incidence angles from 0° to 10° and with blade amplitudes up to 4.2° (for 60Hz). It was found from the experiments that an increased mean incidence caused a higher excitation of the blade from the aerodynamic forces, while the effects of varying the blade amplitudes and frequencies were more difficult to determine. The time-dependent pressures show that the aerodynamic loads are not linear for the stall region. At 6° mean incidence angle, and below, increased blade amplitude for a constant frequency caused the blade suction surface to experience an increased excitation, while for the 7° incidence, and above, the opposite was shown. The fact that the blade amplitude dependence changes when the mean incidence increases above the steady state stall angle is explained by the increased portion of the oscillation cycle spent at stalled conditions. A shift in phase was seen for the highest investigated frequency, which at the time of the experiments was thought to be due to a phase lag between the blade motion and the leading edge vortex, increasing with increasing frequency.

The numerical modelling is based on an implicit finite volume approach with a third order upwind scheme and a Riemann solver. The results showed that flow transition plays a key role in the blade stability during high frequency oscillation, with the transition location influenced not only by incidence angle but also oscillation frequency. With a model varying the transition onset it was possible to predict the phase shift seen in the experiments even for low angles of attack.

Background and Objectives

Flutter of turbomachinery blades is a crucial problem in aircraft propulsion since it reduces the operational envelope of aeroengines and the useful life of their blades. Due to its profound importance blade flutter has been the subject of several investigations [Choudhuri and Knight, 1996; Daube et al., 1985; He and Denton, 1991; Jones and Platzer, 1997] and in recent years significant progress has been made in flutter prediction using Computational Fluid Dynamics coupled with modal structural representation of the blades. The present paper deals with a fundamental problem of aerodynamic stability of turbomachinery blades and attempts to simulate an idealized flutter situation of a thin lifting section. Of central importance is the relationship between the loading of the blade and the flow angle and any phase difference between the two. Furthermore, this paper reveals the demands on CFD for accurately predicting blade flutter both in terms of flow physics and especially turbulence and transition modeling. The current effort builds on previous experimental work by Svensdotter et al. [1997, 1998, 1999, 2000] using transonic flow tunnels and instrumented thin blade sections. It is the objective of this paper to take further the previous experimental and theoretical study using Computational Fluid Dynamics and attempts to shed more light in the fundamental problem of blade stability at transonic flow conditions.
The paper begins with an outline of the experiment and the main conclusions drawn from it and continues with the CFD investigation. Analysis of the obtained results and comparisons against experiments is presented and conclusions are finally drawn along with suggestions for future work.

Description of the Experiment

The wind tunnel used for the experiments was wind tunnel No 5 at Volvo Aero Corporation which is connected to a large air reservoir providing the tunnel with dried air of constant inlet conditions for continuous testing [Kemppainen, 1995]. The test section is 150mm*180mm and is described in detail by Svensdotter et al. [1997]. The inlet Mach number can be varied continuously from 0.3 to 1.6 and the inlet stagnation temperature is about 280K [Johansson, 1992]. The free stream static pressure can be varied between slightly below atmospheric pressure and up to 400kPa at Mach 1. At Mach 0.5 the inlet free-stream turbulence intensity is 1.7% [Kemppainen, 1995].

A symmetrical 2D airfoil NACA 63A006 with a chord length of 80mm and a span of 150mm were used for the tests. The profile is equipped with 13 pressure transducers on the suction surface of the blade. Pressure gauges 1-11 are mounted in cavities connected through drilled holes to the surface (∅ 0.6mm). Gauges 12 and 13 are flush mounted with the surface. The pressure sensors are positioned between 5% and 80% chord. During the tests presented in this paper, sensor 11 was broken and sensor 1 broke during the later part of the test series.

The airfoil is mounted on a shaft with plain bearings in the side walls. The pitching axis through the shaft is at 43% of the chord and the torque was transmitted to the airfoil by the starboard side shaft. Details of the excitation system can be found in Sjunnesson [1992]. The actuator motion can be detected by a high precision potentiometer on the actuator shaft. The blade frequencies and amplitudes can be seen in table 1.

The details of the pressure acquisition system can be found in Svensdotter et al. [1997], as well as discussions concerning the details of the measurement accuracy. The unsteady pressure measurements are performed with an accuracy of ±300Pa, which gives an error in $\tilde{C}_p$ of between ±7 and ±15% of maximum pressure amplitude, considering an error in the blade motion of ±0.05°. The wind tunnel and the experimental setup can be found in Figure 1.

To achieve the objectives outlined in the previous section, the following experimental approach was selected. The investigated flow conditions were specified to consist of high oscillating frequencies (up to 210Hz), from attached to above stall conditions. The inlet Mach number was 0.5 and the chord based Reynolds number was 850 000. The details of the oscillation data selected for discussion in the presented study can be found in Table 1.

For the frequencies used in the presented investigation, f=60Hz corresponds to k=0.09, f=110Hz to k=0.16 and f=210Hz to k=0.31 respectively. The maximum error in reduced frequency is determined to ±0.01.

The unsteady pressure signals were analysed in terms of the amplitude of the perturbation $\tilde{C}_p$ and the phase difference between the pressure signal and the blade motion. The phase angle is positive when the pressure leads the blade and this gives an energy transfer into the blade, i.e. the blade is excited. The amplitude of $\tilde{C}_p$ gives the size of the exciting forces. The measured data is treated with a fast Fourier transform and the amplitude and phase of the unsteady pressure coefficient is based on the first harmonic (Y) of the perturbation $\tilde{C}_p$, according to:

$$Y = \left(\tilde{C}_{pr1} + i\tilde{C}_{pi1}\right)e_1^{i\omega t} \qquad [1]$$

$$\left|\tilde{C}p\right| = \sqrt{\mathrm{Im}(Y)^2 + \mathrm{Re}(Y)^2} \qquad [2]$$

$$\varphi = \arctan\left(\frac{\mathrm{Im}(Y)}{\mathrm{Re}(Y)}\right) \qquad [3]$$

Having achieved the phase angle for both blade movement and pressure signal, the phase difference with the pressure leading the blade, is given by:

$$\Phi = \varphi_p - \varphi_b \qquad [4]$$

For the pressure signal, the interpretation of a separation start is when the pressure sensors show a rapid increase in pressure, less lifting force and disorder in the periodic reading. Again it should be pointed out that the presented analysis is only performed for the suction side, not for the entire blade surface. Due to this, the stability is evaluated in terms of local C_p, instead of C_m.

Defining a damping coefficient according to:

$$\Xi = \frac{1}{c^2} \sum \vec{r} \bullet \Delta\vec{s} \bullet \left|\tilde{C}_p\right| \bullet \sin(\Phi) \qquad [5]$$

gives information of the total damping of the blade suction side, following definitions by Verdon and Usab [1985]. The damping is proportional to the imaginary part of $|\tilde{C}_p|$ ($\left|\tilde{C}_p\right| * \sin(\Phi)$), $\Delta\vec{s}$ represents the area segment where the force of the unsteady pressure is working and $\vec{r}$ is the momentum vector pointing from the pitching point to the surface (in this case the pressure tapping position), all non-dimensionalised with c^2. A negative sign of the damping coefficient means that the blade suction side is excited. Since the total amount of pressure sensors are only 12, 7 upstream the pivot axis and 5 downstream, this is a very course method, but it is considered enough to give information concerning the tendencies at a shock-free flow.

Mathematical Model

A detailed description of the numerical method employed for the solution of the governing equations can be found in Barakos and Drikakis [1998, 1999]. A brief description of the algorithm is given below.

The present method solves the conservation equations of mass, momentum and energy along with the turbulence-transport equations using a finite volume approach and body-fitted curvilinear coordinates. A third-order upwind scheme in conjunction with a Riemann solver [Eberle, 1987; Barakos and Drikakis, 1998] is used for discretising the inviscid fluxes. Limiters based on the squares of pressure derivatives have been used for detecting shocks and contact discontinuities. The viscous terms are discretised by central differences.

Careful consideration has been given to the method used for the time integration of the equations. The time discretisation can be obtained by using either implicit or explicit schemes, and their efficiency is strongly dependent on the time scales imposed by the prescribed motion of the solid boundaries. Both explicit and implicit schemes have been implemented into the present CFD code [Barakos, Drikakis 1998]. In the present study, the implicit version of the method has been employed according to which six or eight equations (in the case of second-moment closure) are solved in a strongly coupled fashion by an implicit-unfactored method which combines Newton sub-iterations and point Gauss-Seidel relaxation. The above implementation improves the robustness of the numerical solution and enables us to achieve convergence in the case of complex turbulence models which contain stiff source terms, e.g. NLEVMs. The method requires a moderate number of Newton iterations ($40 \div 500$, depending on the case) at each time step. In unsteady flows the steady-state solution around a fixed boundary is given as initial condition (see Barakos, Drikakis 1999 for more details). To obtain high values of the CFL number, preconditioning is also performed at each Gauss-Seidel sub-iteration [Barakos, Drikakis 1998]. Several turbulence models are available in the code from simple algebraic closures like the one suggested by Baldwin and Lomax [1978] to full second moment closure Launder and Shima [1989]. Based on past experience

with flows around oscillating aerofoils a non-linear eddy viscosity model of the k-e type was selected. Since only two transport equations are to be solved this model is a good compromise between accuracy and efficiency given the fact that anisotropic stresses are represented in the formulation of the model via a cubic expansion of the Reynolds' stress tensor in terms of the strain and vorticity tensors. The details of the model along with its application to unsteady aerodynamic flows can be found in the works of Barakos and Drikakis [1998, 1999, 2000a, 2000b, 2000c], Craft et al. [1995, 1996] and Suga [1995].

Results and Discussion

A work programme for the CFD computations was initially put in place selecting three test cases out of the ones listed in Table 1. The mean incidence was kept at zero degrees and the amplitude at 4.2 degrees. Three frequencies of oscillations were selected at exactly the same conditions as the experiment.

The employed computational grid was of the C-type with 222 points on the aerofoil, 44 points on each side of the wake and 85 points normal to the profile. Figure 2 presents two views of the grid showing the location of the far-field boundary at 7 chords away from the profile. A zoomed view is also presented on the same figure highlighting the very low thickness of the section and the clustering of points near the leading and trailing edge of the profiles as well as around the wake. Finer grids were also employed without any substantial changes in the obtained results. The final grid was comparable with grid reported in the literature for similar cases [Barakos and Drikakis, 2000a, 2000b, 2000c]. Despite the high Mach number the aerofoil is free from shocks due to its very low thickness; this was especially chosen to approximate compressor blades which in modern designs can be very thin, and there fore more prone to flutter. Typical results of the obtained flowfield are presented in Figure 3 where the density and turbulent kinetic energy fields are shown. Again the aerofoil is free from shocks and one cannot fail to notice the growth of turbulence in the boundary layer of the aerofoil after about 50% of the chord.

The unsteady simulations were performed with sufficient low time step to allow for resolution of the rapid motion of the aerofoil. In all cases the time step employed in computations was two times lower than what Nyqwist's criterion would suggest based on the oscillation frequency. The surface pressure was recorded during the simulation at the same locations as the pressure taps used during the experiment and was subsequently processed at exactly the same way as the experimental results. For the first case of Table 2 results are presented in Figure 4. As can be seen, the time history of the surface pressure is presented for five of the pressure taps and compared against the experiments. The agreement is remarkably good throughout the oscillation cycle. As one moves from the taps near the leading edge towards the trailing edge the clockwise loop of the pressure changes to counterclockwise and in addition, the experimental data tend to be noisier indicating a more turbulent flow field. The comparison of

the phase and amplitude of the experimental and simulation results is presented in Figure 5. Again the agreement is excellent and the results suggest a stable flow configuration.

Further calculations have been performed for the 110 Hz of oscillation frequency and the results are again presented in Figure 6 and Figure 7 for the time domain and frequency domain comparisons, respectively. Although the frequency was doubled the overall characteristics of the pressure history plots remain the same with taps near the leading edge exhibiting a substantial hysteresis, as indicated by the thickness of the loops.

Near the pivot axis the hysteresis is reduced and it becomes again significant towards the trailing edge but this time the history loop is counter-clockwise. The frequency domain plots again suggest a stable flow configuration and further highlight the good agreement between experiments and simulation.

For the highest frequency attempted during experiments calculations have also been undertaken and results are again cross-plotted in Figure 8 and Figure 9. The comparison was rather disappointing given the good agreement obtained for lower oscillation frequencies. As shown the CFD results failed to capture the amount of hysteresis measured during experiments and the change of phase angle between the loading of the blade and the geometric incidence. This failure triggered a set of further calculations detailed on Table 3 where the level of freestream turbulence used in the CFD simulations was varied as well as the oscillation frequency. Levels of freestream turbulence between 0.001 and 1% of the kinetic energy per unit mass of the freestream were employed. The highest oscillation frequency attempted was 420 Hz. Despite these changes the simulation continued to predict a pressure variation in phase with the incidence angles.

In a second attempt to alleviate this discrepancy it was decided to trip the boundary layer at 50% of the chord. This was suggested based on experimental observation of flow transition by Svensdotter et al. [1999] and Svensdotter [1998] and the fact that for the low frequency cases the experimental pressure signals indicated turbulent flow downstream of the pivot axis. In addition to the flow trip calculations at higher mean incidence angles were attempted expecting that possible flow separation may be responsible for the phase change.

Figure 10 presents the time history of taps one, six and nine along with the time history of the imposed incidence angle for a mean incidence of 7 degrees and one degree amplitude of oscillation. Figure 10a corresponds to fully turbulence calculations while Figure 10b presents the results of the tripped flow assumption. As shown, for this case taps near the leading edge of the profile are out of phase with respect to the angle but without the flow trip this is restricted to the first and second probes. Figure 10b suggests that all probes are out of phase with the

incidence and thus flow transition may be central to the correct simulation of the experiment.

To clarify the relative importance of the mean incidence angle and the role of transition further calculations have been performed for a lower mean incidence of 4 degrees keeping the flow trip activated. The results are shown in Figure 11 and as can be seen most of the pressure taps are again out of phase with the angle. This set of calculations suggested that the mean incidence plays a secondary role and the phase change is mainly dictated by the transition of the boundary layer. Further reduction of the mean incidence was attempted this time returning to the conditions of Table 2. Again the trip was kept at 50% of the chord and calculations were repeated for 110Hz and 210Hz of oscillation frequency. For this last case results are presented in Figure 12. Figure 12a suggests that the flow trip has now altered the low frequency results and some of the pressure taps are now out of phase with the incidence. The situation is still favourable for the 210Hz case with all taps maintaining their out of phase characteristics.

Based on the above simulations it is now evident that flow transition plays a key role in the stability of the blade during the forced oscillation at high frequency. However, the way transition was applied was very crude fixing the transition point without allowing for any movement of it with the mean angle. For all calculations a simple sigmoid function was employed taking the intermittency of the flow from zero to one within 3% of chord. This means that placing the transition trip at 50% resulted in fully turbulent flow field at 53% of the chord. In reality a better transition model should be employed which will allow the transition point to move forward at higher incidence angles stabilizing the flow and backwards at lower incidence angles de-stabilising the boundary layer. Different transition points should be employed on the upper and lower surfaces.

Conclusions and suggestions for future work

Numerical simulation has been undertaken for the experiments by Svensdotter et al. [1997, 1998, 1999, 2000]. The time histories of all pressure taps around the oscillating NACA63A006 aerofoil were found to be in agreement between experiments and simulation for oscillation frequencies of 60 and 110 Hz. The experiment indicated a change in phase between loading and angle for the 210 Hz cases which was not predicted by numerical simulations. Several attempts were made to alleviate this discrepancy including varying the level of free stream turbulence in the simulation or further increasing the oscillation frequency. No substantial improvement was found. Inspecting the CFD results it was noticed that transition occurs quite late for this particular aerofoil. A transition trip with a crude transition model was therefore put in place and further CFD results indicated that a phase shift between loading and angle was present. The phase shift was more pronounced for cases of high mean incidence angle. Due to the

crude transition model, a phase difference was also observed for some pressure taps for the 110Hz oscillation cases. It becomes evident that further investigation is necessary with a better transition model in order to increase the fidelity of the CFD simulations. This should be assisted by an investigation of the boundary layer development would perhaps give a few clues to determine the cause of the phase angle shift.

Acknowledgements

The experimental study was financed by Försvarets Materialverk, through Volvo Aero Corporation, The Swedish Gas Turbine Centre and the Chair of Heat and Power Technology at the Royal Institute of Technology. Special thanks to Peter Grasbon, for his help with the dynamic pressure data reduction, Lars-Göran Algotsson and Bengt Härling at VAC and Christer Blomkvist and Rolf Bornhed at the Royal Institute of Technology for preparing the test object and for assistance during and after the wind tunnel tests.

Bibliography

Baldwin, B.; Lomax, H.; 1978
"Thin Layer Approximation and Algebraic Model for Separated Turbulent Flow"
AIAA paper 78-257
Barakos, G., Drikakis, D., 2000a
"Investigation of non-linear eddy-viscosity turbulence models in shock-boundary layer interaction"
AIAA J. 38(3), pp. 461-469
Barakos, G., Drikakis D., 2000b
"Numerical Simulation of Buffeting Flows Using Various Turbulence Closures"
International Journal of Heat and Fluid Flow, 21(5-6), pp. 620-626
Barakos, G., Drikakis, D., 2000c
"Separated Turbulent Flows over Maneuvering Lifting Surfaces"
Philosophical Transactions of the Royal Society of London A: Mathematical Physical and Engineering Sciences 358(1777) Issue 15th, pp. 3279-3292
Barakos, G., Drikakis, D., 1999
"An implicit unfactored method for unsteady turbulent compressible flows with moving boundaries"
Computers, Fluids, 28(8), pp. 899-921
Barakos, G., Drikakis, D., 1998
"Implicit-coupled implementation of two-equation turbulence models in compressible Navier-Stokes methods"
Int. J. for Num. Meth. in Fluids , 28(1), pp. 73-94
Choudhuri, P.G., Knight, D.D., 1996
"Effects of compressibility, pitch rate and Reynolds number on unsteady incipient boundary layer separation over a pitching airfoil"
J. Fluid Mech., , 308, pp. 195-217
Craft, T.J., Launder, B.E., Suga, K., 1996
"Development and application of a cubic eddy-viscosity model of turbulence"
Int. J. Heat Fluid Flow , 17(2), pp. 108-115
Craft, T.J., Launder, B.E., Suga, K., 1995
"A non-linear eddy-viscosity model including sensitivity to stress anisotropy"
Proc. 10th Symposium on Turbulent and Shear Flows, pp. 23-19~-~23-24
Daube, O., TaPhuoc, L., Monnet, P., Coutanceau, M., 1985
"Ecoulement instationaire décollé d'un fluide incompressible autour d'un profile d'aile: une comparaison théorie - expérience"
AGARD Conference Proceedings CP-386, Paper No. 3, in French.
Eberle, A., 1987
"Characteristic flux averaging approach to the solution of Euler's equations"
Lecture No. 1987-04 in VKI series in computational fluid dynamics, VKI
Fan, S., Lakshminarayana, B., Barnett, M., 1993
"Low-Reynolds-number k-ε model for unsteady turbulent boundary-layer flows",
AIAA J. 31(10), pp. 1777-1784
He, L.: Denton, J.; 1991
"An experiment on Unsteady Flow Over an Oscillating Airfoil"
ASME 91-GT-181
Jiang, Y.T., Damodaran, M., Lee, K.H., 1997
"High-resolution finite volume computation of turbulent transonic flow past airfoil"
AIAA J. 35(7), pp. 1134-1142
Johansson, U.; 1992
"Instationära luftkrafter, 2D profil NACA 63A006. Etapp 1, Stationära mätningar."
Internal report Volvo Aero Corporation 9370-532, in Swedish
Jones, K.; Platzer, M.; 1997
"On the Prediction of Dynamic Stall Onset on Airfoils in Low Speed Flow"
8:th International Symposium on Unsteady Aerodynamics of Turbomachines, 1997, Stockholm
Kemppainen, A.; 1995
"Experimental Observations and Numerical Calculations on an Oscillating 2D NACA63A006 Blade"
Licentiate thesis, ISRN KTH/KRV/R-95/4-SE, Royal Institute of Technology, Stockholm
Launder, B.E., Shima, N., 1989
"Second-moment closure for the near-wall sublayer: development and application"
AIAA J. 27(10), pp. 1319-1325
Sjunnesson, I.; 1992
"Experiments on an oscillating 2D aerofoil, NACA 63A006. Test of oscillating system.
Preliminary results" *Internal report VAC 6825-229*
Sorenson, R.L., 1980
"A computer program to generate two-dimensional grids about airfoils and other shapes by the use of Poisson's equation"
NASA Technical Memorandum 81198
Spalart, P.R., Allmaras, S.R., 1992
"A one-equation turbulence model for aerodynamic flows"
AIAA Paper 92-0439
Suga, K., 1995

“Development and application of a non-linear eddy viscosity model sensitized to stress and strain invariants”
PhD Thesis, University of Manchester Institute of Science and Technology
Svensdotter, S.; 1998
“Investigation of Boundary Layer Transition for Transonic Flow over Compressor and Turbine Airfoils”
Doctoral Thesis, The Royal Institute of Technology, Stockholm, Sweden, ISBN-91-7170-348-9
Svensdotter, S.; Hu, J.; Fransson, T.; 1999
“Transition studies on a NACA63 isolated airfoil at High Mach numbers”
3:rd European Conference on Turbomachines, IMechE -99, C557-159
Svensdotter, S.; Johansson, U.; Fransson, T.; 2000
“Parametric Study of the Pressure Stability on an Oscillating Airfoil from Stable to Stalled Flow Conditions”
ASME 2000-GT-384
Svensdotter, S.; Johansson, U.; Fransson, T.; 1998
“Unstable Lift on an Oscillating Blade at Near Stall Conditions”
AIAA 98-3749, submitted to the AIAA Journal of Propulsion
Svensdotter, S.; Johansson, U.; Kemppainen, A.; Fransson, T.; 1997
“Correlation of Pressure and Hot Film Data on an Oscillating 2D NACA63A006 Single Airfoil at High Incidence”
8:th International Symposium on Unsteady Aerodynamics of Turbomachines, 1997, Stockholm
Verdon, J.; Usab, W.; 1985
"Application of linearized unsteady aerodynamic analysis to standard cascade configurations"
NASA Contractor Report, UTRC Report R85-956896-4
Walraevens, R.; Cumpsty, N.; 1995
“Leading Edge Separation Bubbles on Turbomachine Blades”
Journal of Turbomachinery, January 1995, Vol. 115, pp. 115 - 125

Figures

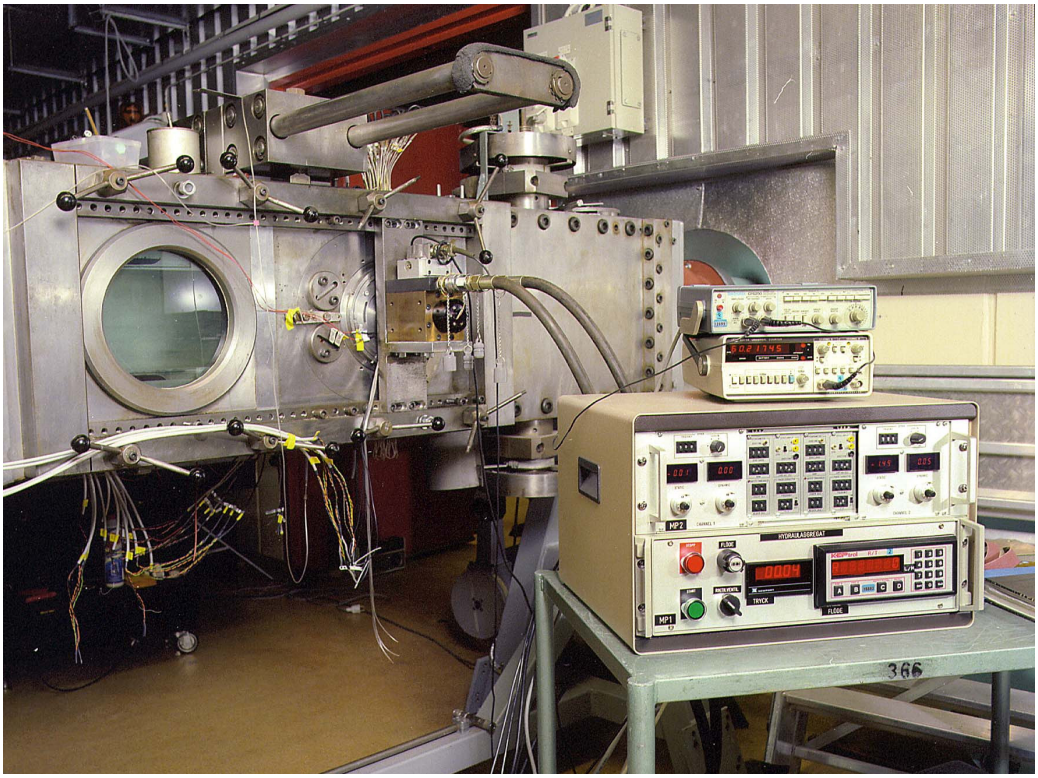

(a)

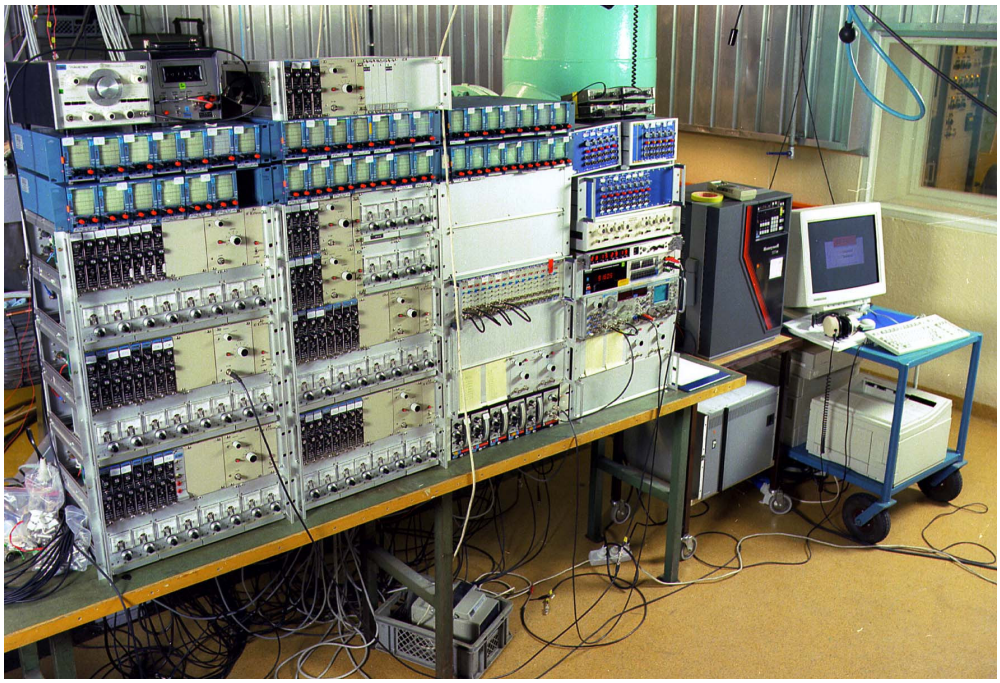

(b)

Figure 1 Photograph of the employed wind tunnel (a) and the measuring equipment (b).

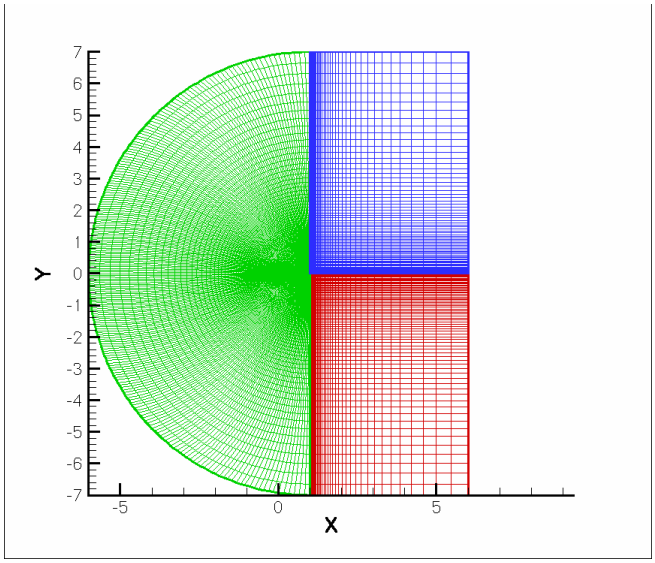

(a)

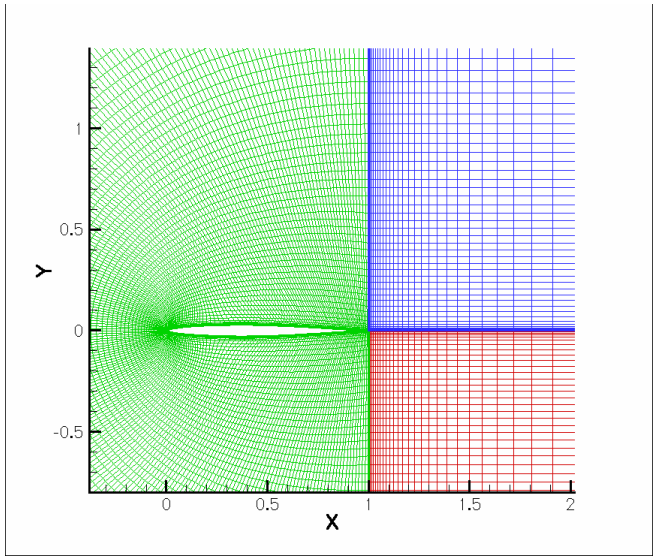

(b)

Figure 2 (a) Three-block grid used in calculations and (b) zoomed view around the aerofoil.

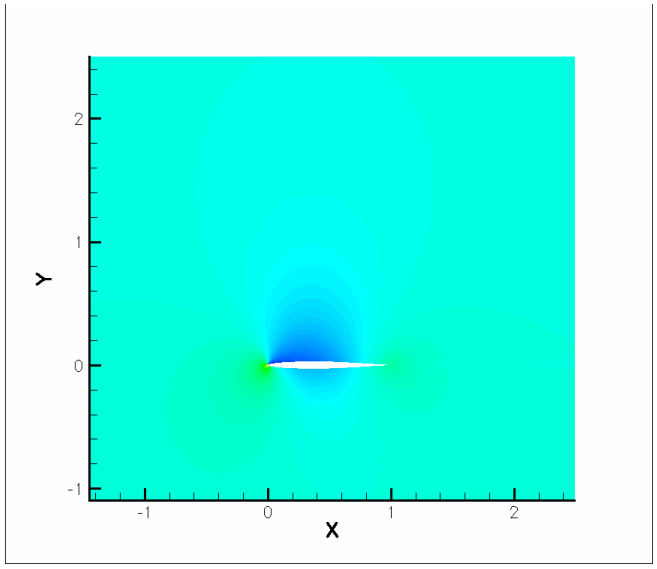

(a)

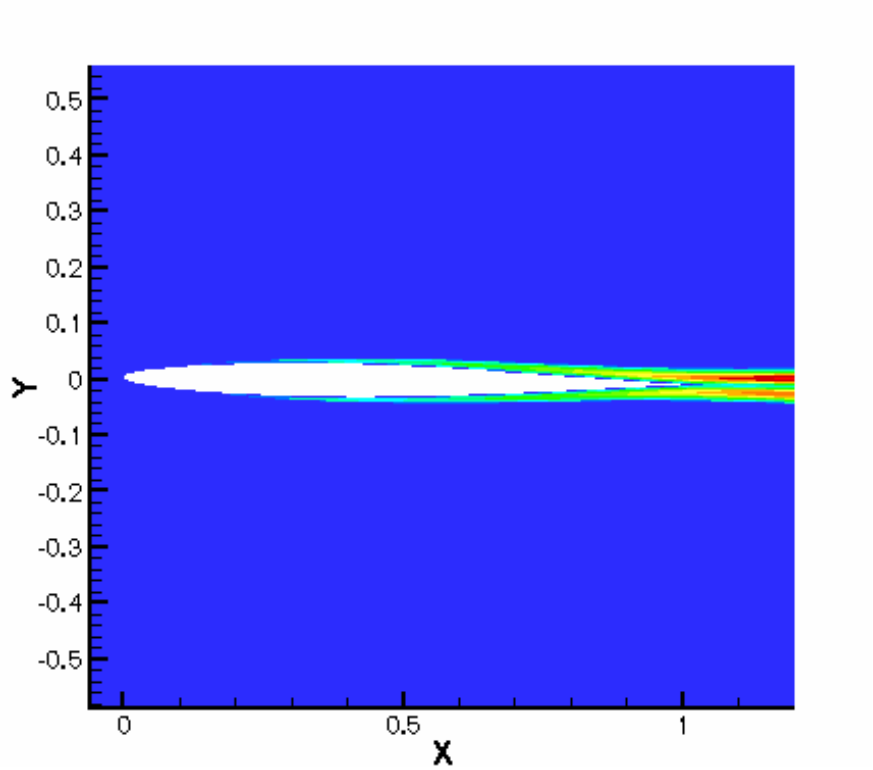

(b)

Figure 3 Indicative results for the flow around the NACA 63A006 aerofoil (a) density and (b) Turbulent kinetic energy at Re=850 000, M=0.5, α=0.

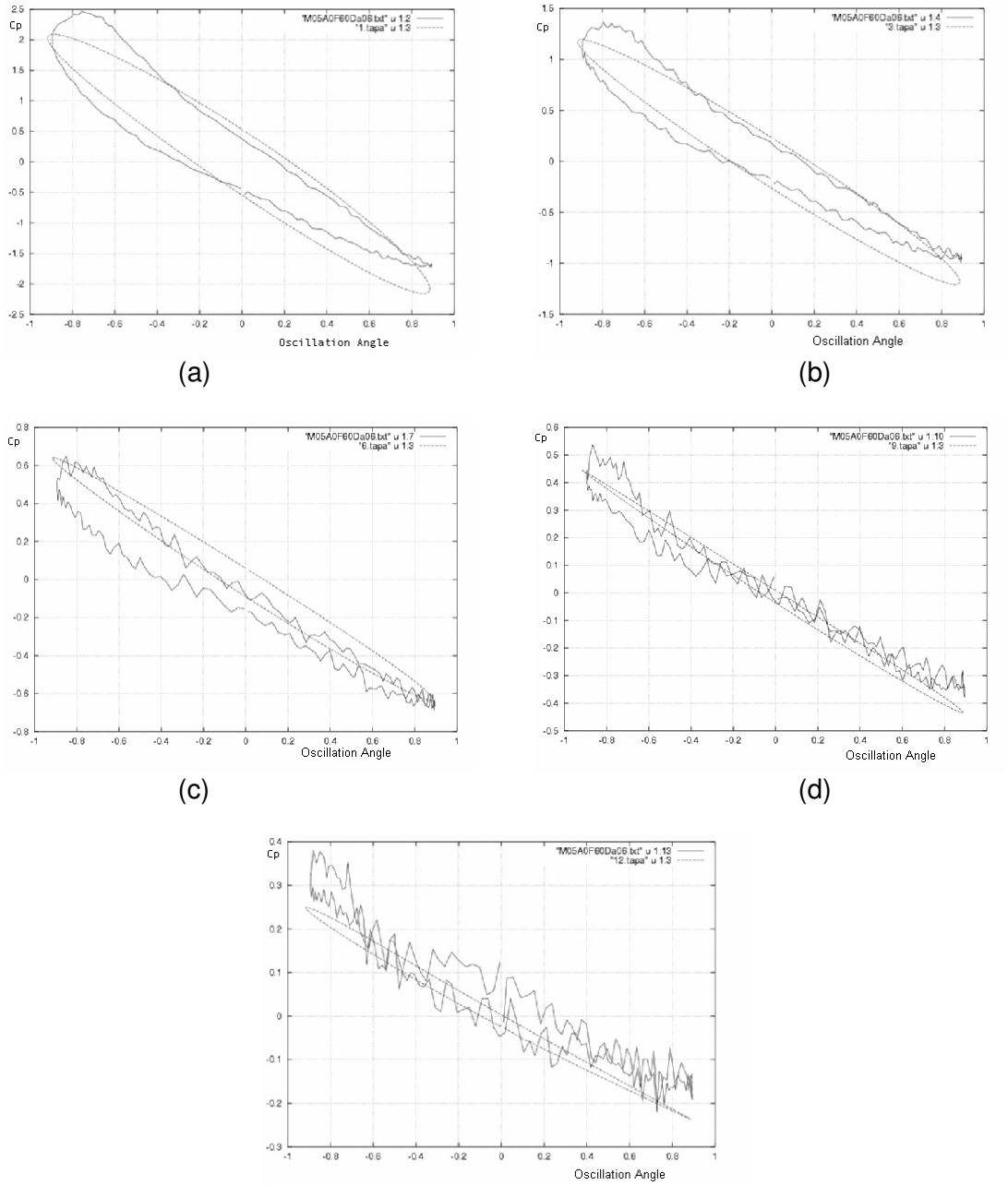

Figure 4 Comparison between experiment and simulation for the 60 Hz oscillation case. Cp versus angle loops are presented for five pressure taps.

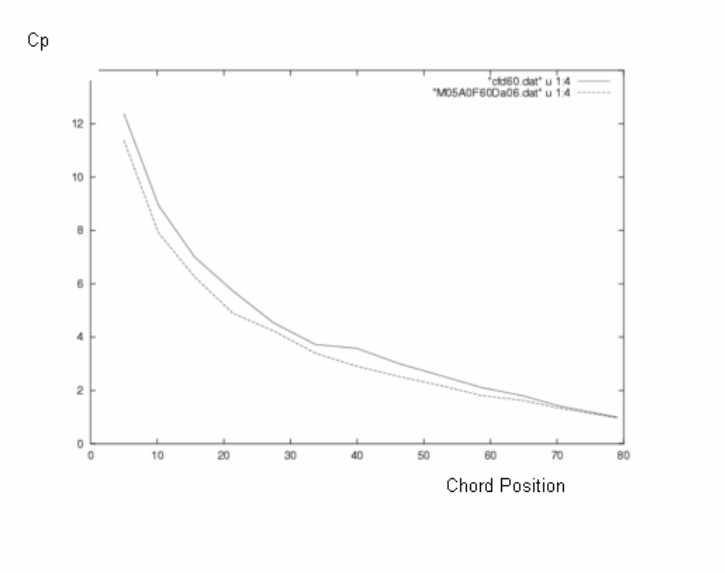

(a)

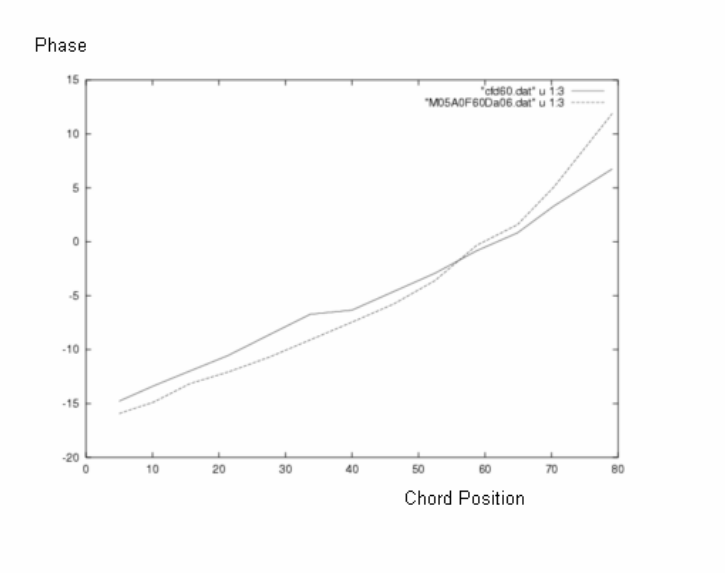

(b)

Figure 5 Comparison between experiment and simulation for the 60 Hz case. (a) amplitude and (b) phase for all pressure taps on the aerofoil.

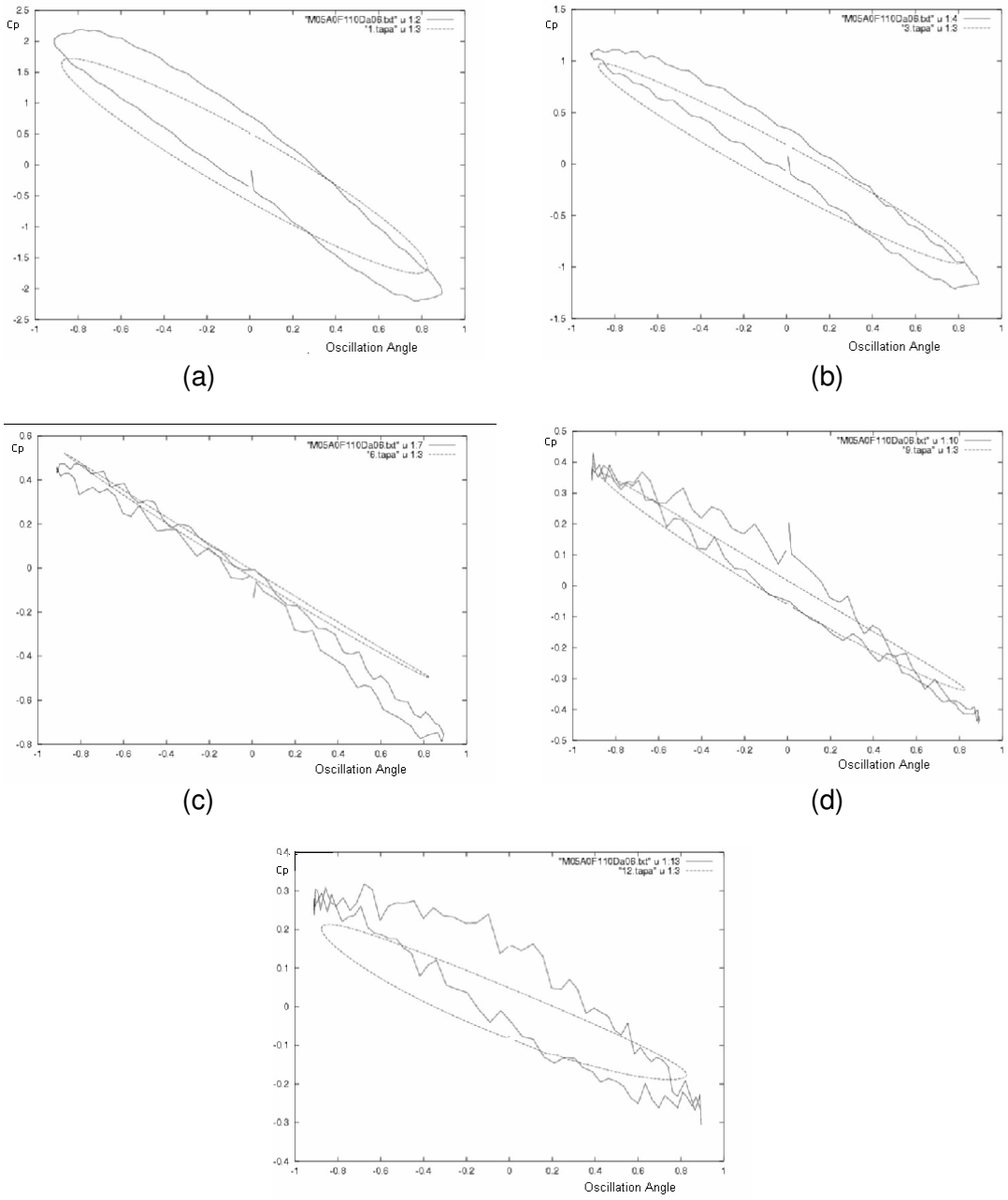

Figure 6 Comparison between experiment and simulation for the 120 Hz oscillation case. Cp versus angle loops are presented for five pressure taps.

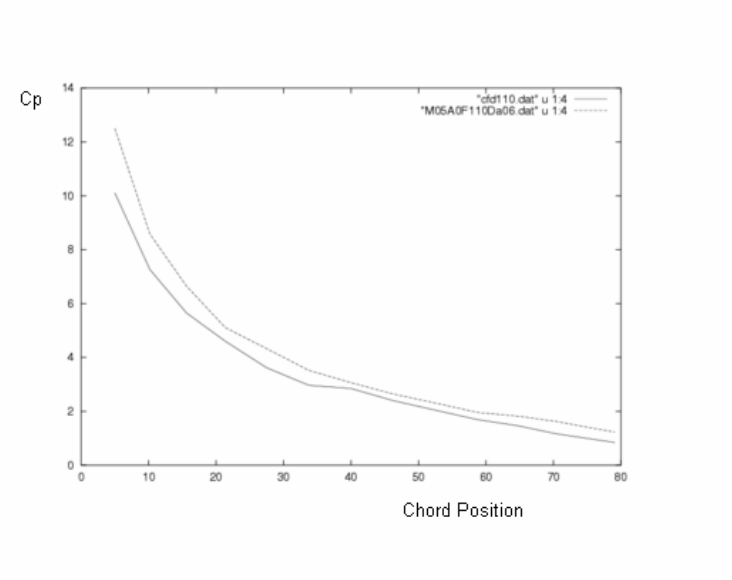

(a)

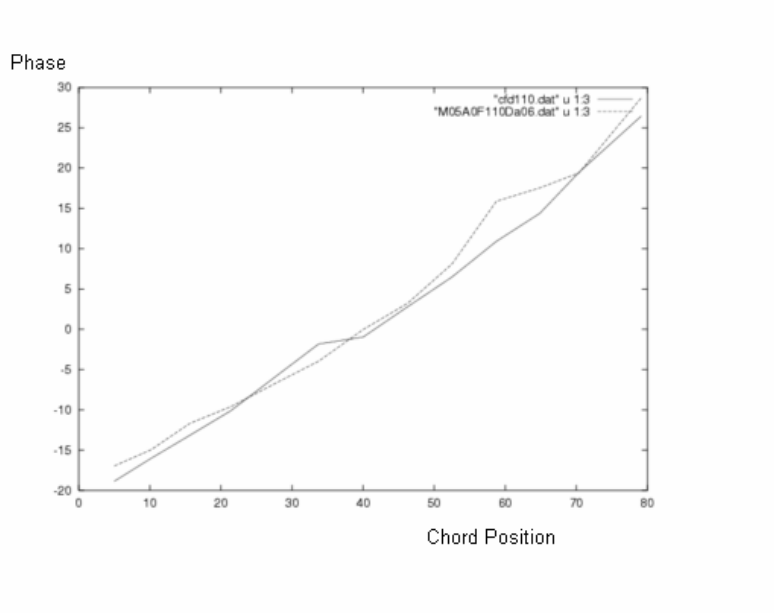

(b)

Figure 7 Comparison between experiment and simulation for the 120 Hz case. (a) amplitude and (b) phase for all pressure taps on the aerofoil.

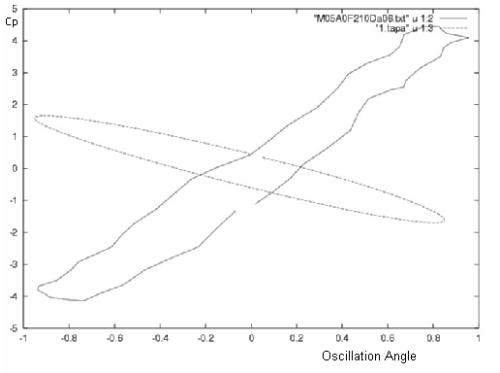

(a)

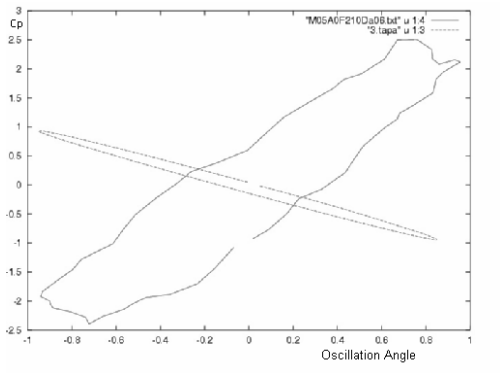

(b)

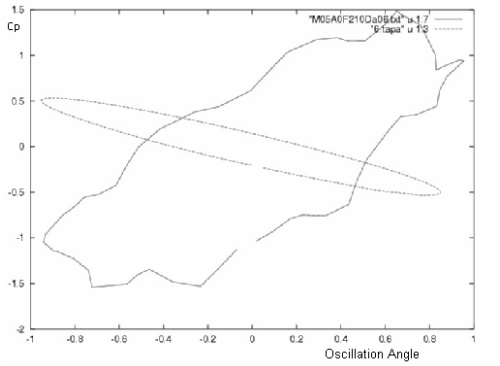

(c)

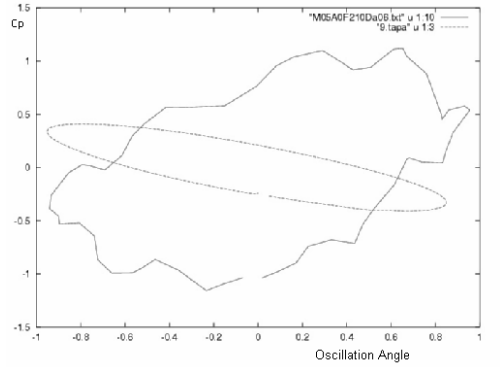

(d)

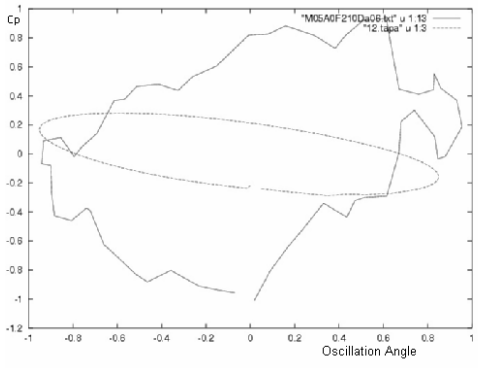

(e)

Figure 8 Comparison between experiment and simulation for the 210 Hz oscillation case. Cp versus angle loops are presented for five pressure taps.

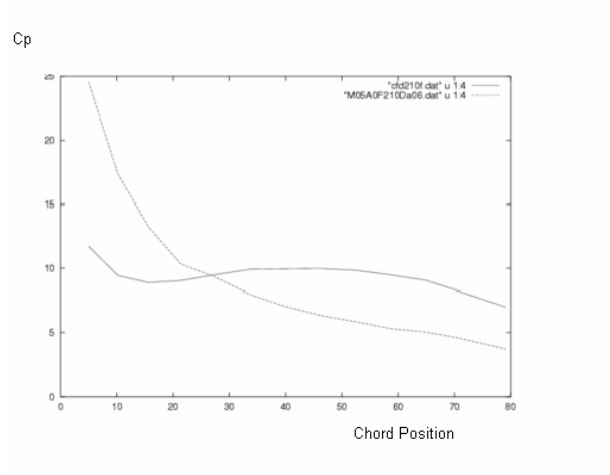

(a)

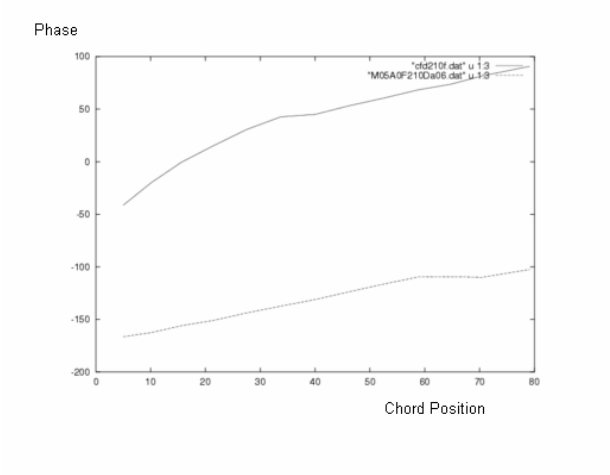

(b)

Figure 9 Comparison between experiment and simulation for the 210 Hz case. (a) amplitude and (b) phase for all pressure taps on the aerofoil.

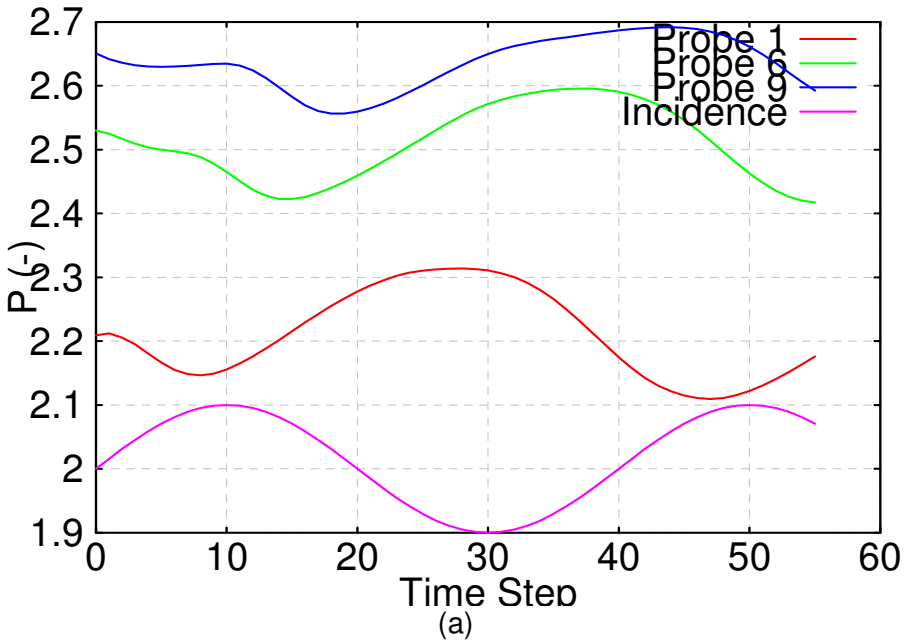

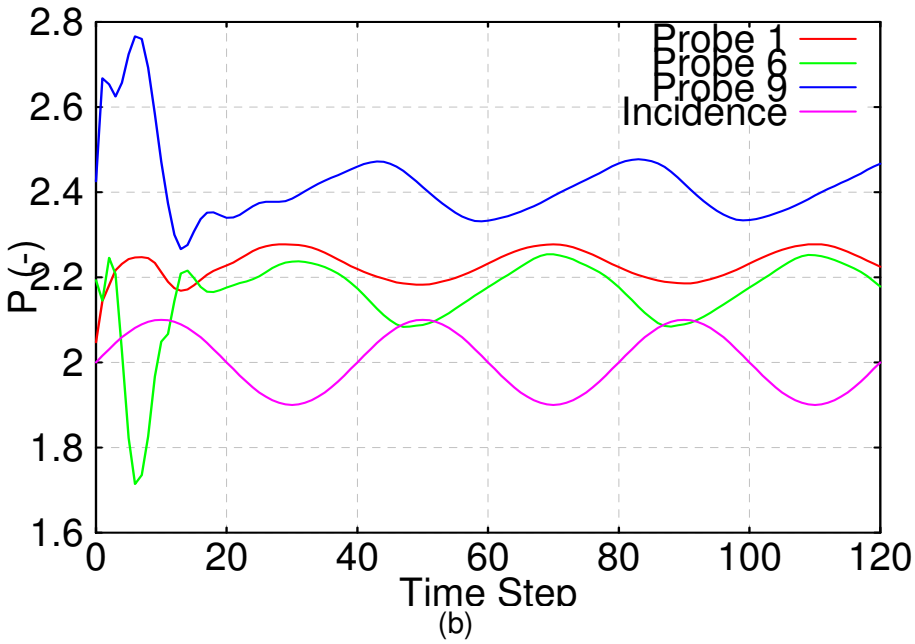

Figure 10 Pressure and incidence history (a) Mean incidence 7 degrees, Amplitude 1 degree, Frequency 210 Hz and (b) Mean incidence 7 degrees, Amplitude 1 degree, Frequency 210 Hz. The boundary layer was tripped at 50% of the chord for cases (b).

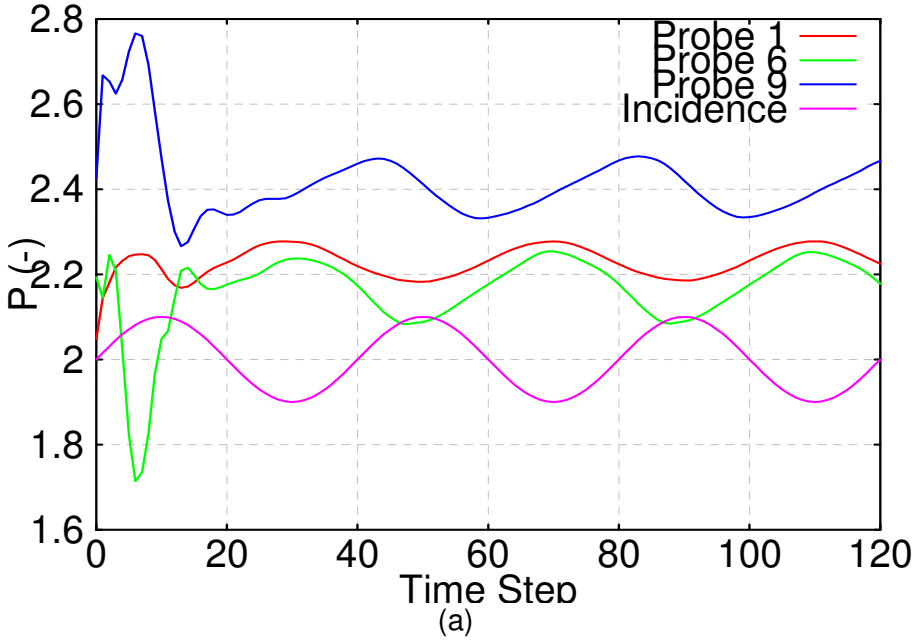

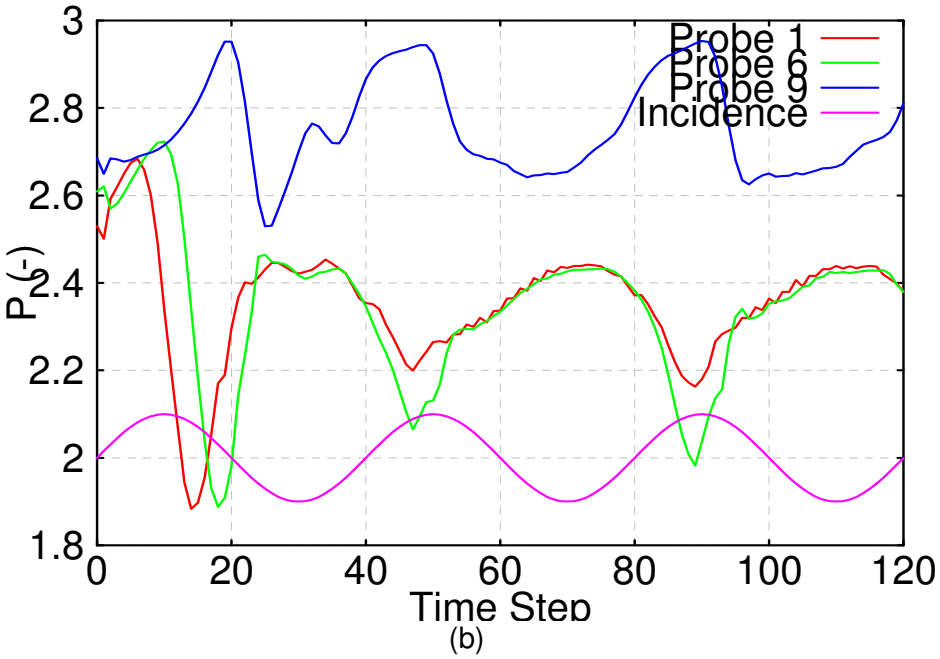

Figure 11 Pressure and incidence history (a) Mean incidence 7 degrees, Amplitude 1 degree, Frequency 210 Hz and (b) Mean incidence 4 degrees, Amplitude 1 degree, Frequency 210 Hz. The boundary layer was tripped at 50% of the chord for both cases.

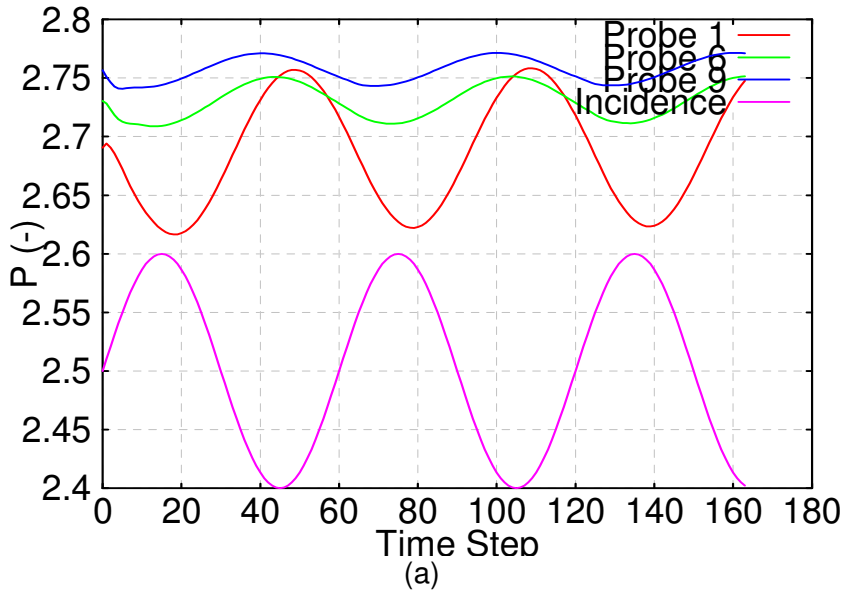

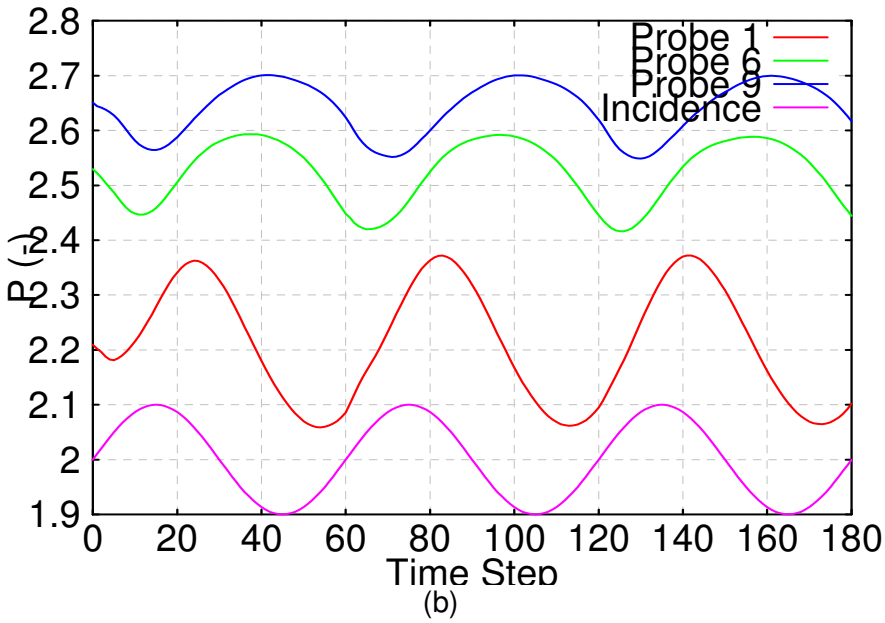

Figure 12 Pressure and incidence history (a) Mean incidence 0 degrees, Amplitude 1 degree, Frequency 210 Hz and (b) Mean incidence 0 degrees, Amplitude 1 degree, Frequency 120 Hz. The boundary layer was tripped at 50% of the chord for both cases.

Tables

α [°]	$\hat{\alpha}$ [°] 4.2	2.7	0.8
0	60Hz	60Hz	60Hz 110Hz 210Hz
1	60Hz	60Hz 110Hz	60Hz 110Hz 210Hz
3	60Hz	60Hz 110Hz	60Hz 110Hz 210Hz
6	60Hz	60Hz 110Hz	60Hz 110Hz 210Hz
7	60Hz	60Hz 110Hz	60Hz 210Hz
9	60Hz	60Hz 110Hz	60Hz 110Hz 210Hz
10	60Hz	60Hz 110Hz	60Hz 110Hz 210Hz

Table 1 Summary of test conditions for the wind tunnel experiments.

Frequency	60Hz	110Hz	210Hz
Inlet mach No.	0.5	0.5	0.5
Inlet stagnation temperature	280K	280K	280K
Reynolds number	850 000	850 000	850 000

Table 2 Summary of conditions for the selected baseline cases for CFD calculations.

Case A	Reference Case 210Hz
Case B	Free-stream turbulence 1%
Case C	As Reference at twice the frequency
Case D	As Reference with free-stream turbulence 0.001%
Case E	Twice the frequency and turbulence 0.001%
Case F	Four times the frequency

Table 3 Summary of conditions for further cases attempted at 210Hz of oscillation frequency.